

Dynamic Single-Input Control of Multistate Multitransition Soft Robotic Actuator

Geron Yamit, Ben-Haim Eran, Gat D. Amir, Or Yizhar, and Givli Sefi*

Soft robotics is an attractive and rapidly emerging field, in which actuation is coupled with the elastic response of the robot's structure to achieve complex deformation patterns. A crucial challenge is the need for multiple control inputs, which adds significant complication to the system. A novel concept of single-input control of an actuator is proposed, which composes of interconnected bistable elements. Dynamic response of the actuator and predesigned differences between the elements are exploited to facilitate any desired multistate transition using a single dynamic input. Formulation and analysis of the control system's dynamics and pre-design of its multiple equilibrium states, as well as their stability, are shown. Then, fabrication and demonstration are done experimentally on single-input control of two- and four-element actuators, where the latter can achieve transitions between up to 48 desired states. This work paves the way for next-generation soft robotic actuators with minimal actuation and maximal dexterity.

1. Introduction

Robots that carry out complicated tasks, such as dexterous robots for medical procedures, articulated robotic arms for manipulation and grasping tasks, or snake-like robots for search-and-rescue missions in cluttered environments, must rely on multiple degrees of freedom (DOFs). The inherent complexity associated with the coordinated control of a large number of actuators poses major difficulties and limitations in terms of structural intricacy and energy expenditure. This has become a crucial bottleneck in the development of modern robots, and therefore efforts are being invested to develop methods that enable controlling over several DOFs by means of a small number of inputs (e.g.,^[1,2]). The ideal visionary solution to this challenge would be devising a way to dictate any desired trajectory of a system comprised from several DOFs, with only one controlled input. We show that such fantastic ability, although seeming


unrealistic at first glance, can be achieved using cleverly designed multistable structures and exploiting their unique dynamic behavior.

Currently, most dexterous robots considered in the literature, such as those mentioned earlier, are conventionally composed of rigid links connected by actuated joints.^[3,4] For interaction involving intermittent contact with objects and human-robot collaboration, the operation of such robots requires highly complicated control that involves force-sensing and coordination between multiple joints, as well as feedback stabilization. A promising remedy lies in the rapidly evolving field of *soft robotics*, in which actuation is coupled with the elastic response of the robot's structure to achieve complex continuous deformation patterns.^[5–18] Soft actuators are utilized

for various robotic applications,^[19–23] such as bio-inspired legged locomotion,^[6,24,25] aquatic locomotion,^[26] soft grippers,^[27,28] deformable sheets,^[29–31] and distributed sensing.^[32–34] Several actuation methods exist for soft actuators, such as control of flow rate or pressure in channel network or bladders embedded within an elastic structure,^[35–39] electrostatic and piezo-electric activation of smart materials,^[27,40–43] magnetic field,^[44–48] thermal and thermo-chemical activation,^[49–56] and more.

A crucial challenge in soft actuators is the typical need for multiple control inputs, which must be coordinated and involve closed-loop feedback and sensing. This may impose significant technical complications, limiting the realization of the control system. Moreover, accurate tracking of continuous time-varying deformation trajectories of an inertial-elastic structure using feedback control may also require high energy expenditure. A key concept which has been introduced for actuation of soft structures is the use of *bistable elements*. A bistable element is characterized by two distinguished stable equilibrium configurations for the same prescribed load, separated by an unstable (spinodal) equilibrium state. Such behavior can be observed in curved beams,^[57–61] thin-walled hyperelastic balloons,^[1,62–64] and prestressed elastic sheets.^[65–75] An actuator made of multiple interconnected bistable elements can transition between multiple stable states using minimal activation for snapping each element, while the rest of the motion is done passively.^[76–83] This enables achieving complex motions using minimal actuation energy by exploiting the multistable energy landscape of the system.^[84–91] For example, an actuator containing N bistable elements, can provide a multitude of possible trajectories that involve transitions between 2^N stable states. This concept has

G. Yamit, B.-H. Eran, G. D. Amir, O. Yizhar, G. Sefi
Faculty of Mechanical Engineering
Technion –Israel Institute of Technology
Haifa 32000, Israel
E-mail: givli@technion.ac.il

 The ORCID identification number(s) for the author(s) of this article can be found under <https://doi.org/10.1002/aisy.202500077>.

© 2025 The Author(s). Advanced Intelligent Systems published by Wiley-VCH GmbH. This is an open access article under the terms of the Creative Commons Attribution License, which permits use, distribution and reproduction in any medium, provided the original work is properly cited.

DOI: 10.1002/aisy.202500077

been exploited in fluid-actuated soft robotic actuators,^[64,84,92,93] electrically and magnetically actuated actuators,^[94–96] for applications such as energy harvesting,^[97,98] robotics,^[2,99–101] micro-electro-mechanical systems,^[102] energy absorption,^[103] metamaterials,^[104,105] folding of actuated origami sheets,^[106–110] and more. The main limitation of this concept is the need to actuate each of the bistable elements by a separate controlled input, which is still complicated.

In order to minimize the complexity of the control system for multistable actuators, the concept of *single-input control* has been recently introduced. According to this concept, the bistable elements are interconnected and mechanically coupled. Moreover, the elements differ in their mechanical properties in a pre-designed way that enables dictating the order of transitions between multistable states of the actuator. This concept has been demonstrated in single-input control by.^[111,112] In these works, the actuator was able to produce only specific sequences of state transitions. Also,^[92] proposed multi-material viscoelastic architected materials whose snapping sequence can be tuned using temperature as a control parameter. The work of^[41] presented single-input flow rate control of a chain of serially connected hyper-elastic rubber balloons, where it was shown that it is possible, in principle, to reach all possible 2^N states. However, the *sequences of transitions* from initial to target state were limited to a specific order, which may result in very long sequences. In a recent work,^[106] presented an actuator consisting of serially connected bistable cells with pre-tuned magnetization, which are actuated by an external magnetic field. While this actuator is able to transition directly between any desired stable states, it requires control of both the magnetic field's magnitude and direction, which are effectively two scalar inputs. Also, the use of

high-energy magnetic fields is often not allowed in applications that involve sensitive electronics or optical components.

While all the actuators mentioned earlier rely on quasi-static changes of the states using slow input rate, we propose here a novel concept of *exploiting the system's dynamics* in order to enable all possible transitions between neighboring multistable states using a single input. Moreover, careful design of the potential energy profiles of the mechanical bistable elements comprising the actuator, enables achieving added stable equilibrium states where one of the elements lies in its intermediate (spinodal) equilibrium. This enables increasing the number of multistable states for an N -element system up to $2^N(1 + N/2)$, which gives a refined resolution of the actuator's states for the same number of elements.

2. Results

We propose a novel approach that leverages the system's dynamic behavior to enable direct transitions between neighboring multistable states using a single input. This innovative method can be applied to a wide range of mechanical systems across various fields. In this work, we demonstrate it using a system of bistable mechanical beams,^[57–61] as shown in the experimental setup in **Figure 1a**.

In the following, we introduce the physical principles underlying the concept for controlling transitions between different states. We then present an experimental demonstration of a multistate actuator used to control an articulated robot in a laboratory environment. Finally, we provide a theoretical analysis of the actuator to deepen the understanding and complete the research framework.

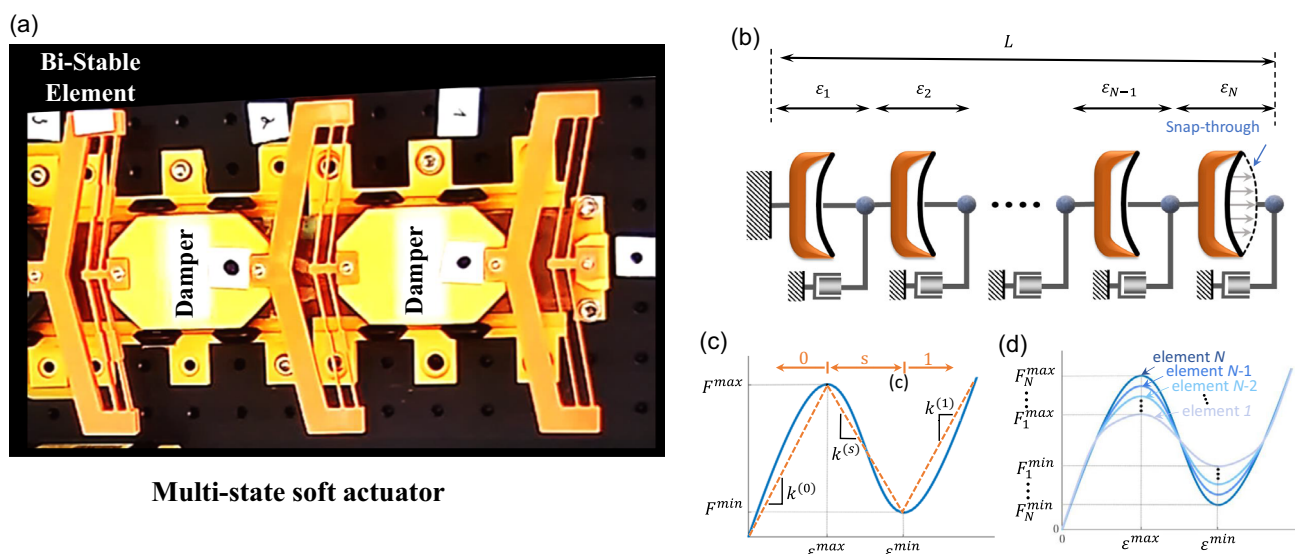


Figure 1. Multistate soft actuator comprised from bistable beams that are connected in series. a) Experimental setup of multistate soft actuator comprised from three bistable beams. b) Schematic illustration of a multistable chain model and notations. c) The force–displacement relation $F(\epsilon)$ of a bistable element with two states of positive stiffness, states '0' and '1', separated by a branch of negative stiffness termed the spinodal region. The tri-linear approximation of this non-monotonic relation, denoted by the dashed straight-line segments, may offer useful analytical insights. d) Pre-designed variability between the bistable elements that makes each element weaker or stronger compared to its neighbors, as described in Equation (1).

2.1. Multistate Soft Actuator

Consider a chain of N bistable elements connected in series, as illustrated in Figure 1b. Each bistable element is characterized by a non-monotonic force–displacement relation $F(\epsilon)$ having two phases of positive stiffness separated by an intermediate branch of negative stiffness, see Figure 1c. In force-control conditions, the branch of negative stiffness, termed *spinodal phase*, is unstable, while the two phases of positive stiffness are stable. Thus, practically, two distinctly separated equilibrium phases are possible, which we denote by ‘0’ and ‘1’, while the intermediate spinodal phase is denoted by ‘s’.

It is straightforward to demonstrate that static equilibrium requires the forces in all elements to be equal. However, due to the non-monotonic force–displacement relationships of the elements, the equilibrium solution is not unique. In other words, multiple equilibrium solutions corresponding to different states may exist for the same prescribed extension. As noted in,^[113] when all elements in the chain are in phase ‘0’ or ‘1’, this configuration is always stable. However, states with more than one element in the spinodal ‘s’ phase are unstable. Intermediate states, where exactly one element is in the ‘s’ phase, are stable only if the actuator’s equivalent stiffness is negative. Although an intermediate (mixed) state involving one element in the spinodal phase (e.g., (10s)) is typically considered unstable, it can be stabilized by altering the relationships between the local stiffnesses of the beam elements. Depending on the desired motion characteristics and the specific application, stable intermediate states can be advantageous, offering an added degree of tunability. Further technical details about this concept can be found also in the Supporting Information.

Accordingly, the chain of bistable elements may be viewed as an actuator with up to 2^N stable equilibrium states (or $2^N(1 + N/2)$ if intermediate states are designed to be stable), each corresponding to a different arrangement of zeros and ones (or ‘s’ if the intermediate state is stable), represented as a binary number. The sequence of transitions between these different binary states defines a trajectory. For example, when $N = 2$, state (11) may be reached through $N! = 2$ different trajectories that begin at state (00), and vice-versa, giving rise to a total of $(N!)^2 = 4$ different complete-cycle trajectories, as follows: $\{(00) \rightarrow (10) \rightarrow (11) \rightarrow (01) \rightarrow (00)\}$, $\{(00) \rightarrow (10) \rightarrow (11) \rightarrow (10) \rightarrow (00)\}$, $\{(00) \rightarrow (01) \rightarrow (11) \rightarrow (01) \rightarrow (00)\}$, $\{(00) \rightarrow (01) \rightarrow (11) \rightarrow (10) \rightarrow (00)\}$.

2.2. Achieving Single-Input Control of Multistate Actuator

We propose to control such a multi-state actuator, that is, to make it follow any desired trajectory, using a single input that controls the total length of the chain, $L(t)$, or particularly, the rate at which its length is changing, $\dot{L} = v(t)$. The concept is based on exploiting two competing symmetry-breaking mechanisms that, together, dictate the next transition event from a given state. This tug-of-war is decided by the rate $v(t)$, which is the only control input. Above, the notion of symmetry refers to the case where all bistable elements are identical, that is, have the same force–displacement relation. Subjecting such a chain to quasi-static

displacement-control conditions would lead to a random sequence of transition events since all elements reach the critical transition force together, that is F^{\max} during extension or F^{\min} during contraction.

Symmetry breaking is achieved through two distinct mechanisms. First, we incorporate pre-designed variability in the bistable elements in an organized manner, which is formulated as

$$F_i^{\max} < F_{i+1}^{\max} \text{ and } F_i^{\min} > F_{i+1}^{\min} \text{ for } i = 1 \dots N - 1 \quad (1)$$

as illustrated schematically in Figure 1d. Second, we introduce dissipative damping into the elements’ motion, adding rate-dependent forces. The damping mechanism can be implemented using a wide range of possible components, including industrial dashpot dampers, rubber-like polymers, pneumatic elements with viscous resistance, magnetic forces, or any other restraining elements that introduce force differences among the elements in transient states. Here, we achieve an amplified damping effect using stationary magnets, in order to enable careful and systematic investigation. Nevertheless, the magnet is not an inherent part of the system and can be replaced by other mechanisms for generating rate-dependent resistive forces.

While the variability breaks the symmetry by making the elements “weaker” or “stronger”, damping makes the actual force experienced by each of the bistable elements different from that of its neighbors. By clever design, we make these two mechanisms compete such that the input rate $v(t)$ dictates the level of dominance between them, and by that, enforce a desired order of transitions.

2.3. Experimental Demonstration

2.3.1. Control of a 3-link Robot Using a 2-element Actuator

In order to demonstrate the concept discussed above, we begin by presenting the results of experiments involving a multi-stable actuator with two bistable elements, $N = 2$. We then show its application in the actuation of a 3-link robot. Here, the number of the stable binary states is four, $\{(00), (10), (01), (11)\}$, and the number of possible trajectories in each direction (from state (00) to (11) or vice-versa) is two, giving rise to an overall of four different complete-cycle trajectories, see Figure 2.

Each bistable element of the soft actuator is made of a double curved-beam structure,^[114,115] which is manufactured by 3-D printing from PLA (see more details in Section 3). Importantly, the bistable behavior of the curved-beam element, for example, its stiffness in different states or the level of forces F^{\max} and F^{\min} , can be tuned by a careful design of the curved-beam geometry. Thus, variability between the force–displacement relations of the two bistable elements was introduced by means of differences in the geometry of the curved-beams (see Section 3).

The two bistable elements are mounted on wheeled carts that move along a rail. Rate-dependent damping is produced by attaching magnets to the bottom of the carts, which interact, without contact, with a copper plate that is fixed to the rail. The relative motion of the magnets with respect to the copper plate induces an electric field that creates eddy currents in the

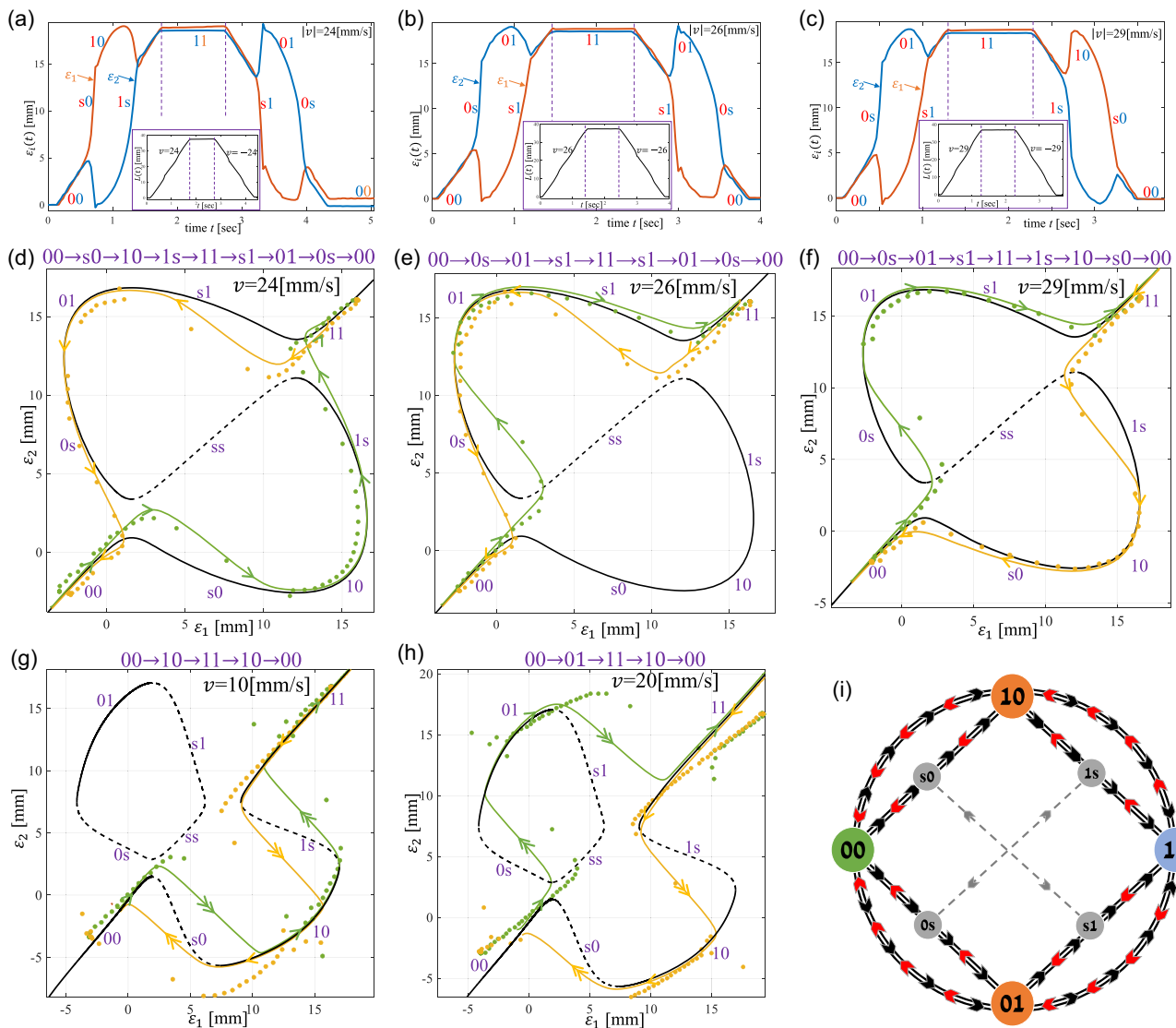


Figure 2. Experimental results of the two-element actuator. a–c) Measured elongations of the elements ε_i versus time t , for input rates $\nu = \{24, 26, 29\} \text{ mm s}^{-1}$, respectively. d–f) Measurements of displacements plotted as dots in the plane of $(\varepsilon_1, \varepsilon_2)$, for input rates $\nu = \{24, 26, 29\} \text{ mm s}^{-1}$, respectively. The three different trajectories demonstrate the ability to follow each of the sequences of state transitions by merely controlling the rate of the input (extension/contraction) rate ν . For reference, the equilibrium curves (solid and dashed black curves for stable or unstable equilibrium, respectively) and the predictions of the numerical simulations of our theoretical dynamic model (orange and green solid curves with arrows) are illustrated as well. g–h) Experiment results with unstable intermediate states. Note the abrupt transitions (snap-through) between binary states, denoted by double-arrows, in contrast to the smooth transition through intermediate states observed in (d–f). i) State transition diagram of a two-element actuator with stable intermediate states.

plate. In turn, a damping force that is proportional to the relative velocity is produced.^[116] Figure 2 shows the results of extension-contraction cycles of the soft actuator performed at different input rates, demonstrating the ability to follow each of the four possible trajectories of state transitions by merely controlling the input rates (see also the Supporting Information Video). As expected, at low rates, the weaker element changes its state before the stronger element. On the contrary, if the input rate is high enough, the damping forces become dominant, causing the stronger element to switch first by changing the distribution of forces along the chain.

State-Transition Control of a 3-link Robot: Since it is possible to follow any of the four complete-cycle trajectories by a single input, the multistable chain can be harnessed to function as an actuator that allows achieving four different cycles with a single-input control. This is demonstrated by connecting a 3-link robot to the multistable actuator with two elements, as shown in **Figure 3**. The 3-link robot is widely used as a basic model of planar locomotion of micro-swimmers,^[117] robotic snake swimmers in ideal fluid,^[118] and inchworm-like crawling.^[119] The important capability to generate locomotion relies on non-reversible undulatory motion of the two joint angles θ_1, θ_2 of the robot

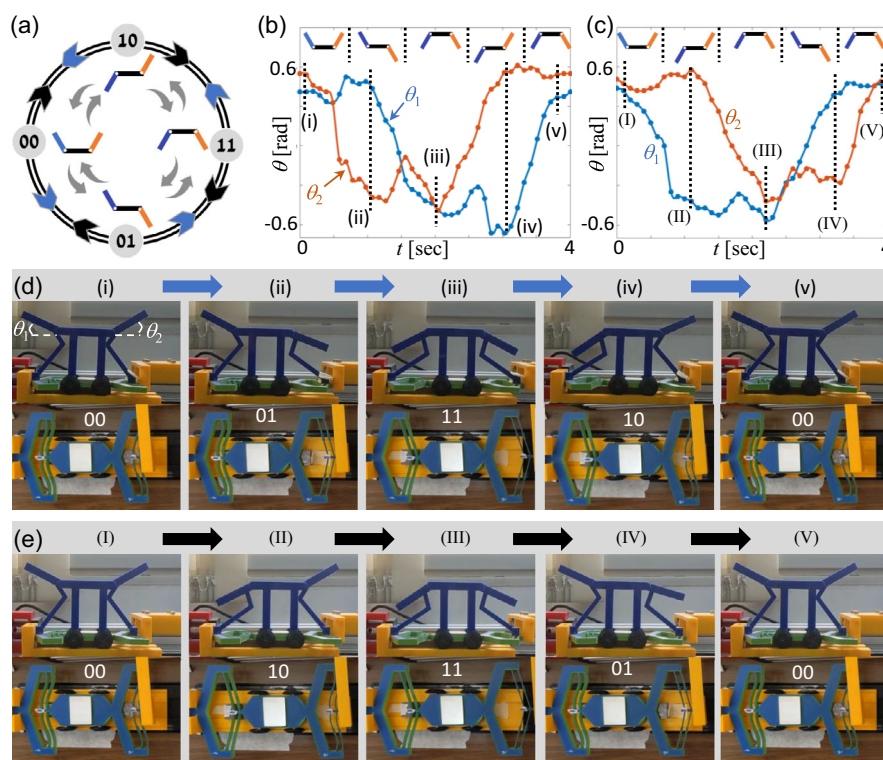


Figure 3. A 3-link robot controlled by a single input using the proposed actuator, allowing for any desired sequence of strokes. a) A transition diagram between binary states of the 3-link robot. b) Plots of measured the robot's two joint angles θ_i versus time t for low input rate $|\nu| = 20 \text{ mm s}^{-1}$, leading to state sequence $\{(00) \rightarrow (01) \rightarrow (11) \rightarrow (10) \rightarrow (00)\}$. c) Plots of measured the robot's two joint angles θ_i versus time t for low input rate $|\nu| = 28 \text{ mm s}^{-1}$, leading to state sequence $\{(00) \rightarrow (10) \rightarrow (11) \rightarrow (01) \rightarrow (00)\}$; Snapshot pictures from the movie of the robot's motion d) for low input rate, e) for high input rate. Below each snapshot sequence, we show illustrations of the bistable states of the actuator's two elements.

in phase-shifted periodic oscillations, which form a discretization of a traveling wave. In contrast to the classical design which requires two separate inputs for controlling the joint angles, using our concept demonstrates that the choice of sequence of strokes of the 3-link robot can be completely controlled by a single input (see also the Supporting Information Video). In particular, it is possible to generate a non-reciprocal “traveling wave” cycle in either direction, by appropriately choosing the rate of the single input, as shown in Figure 3b,c.

2.3.2. Multi-State Multi-Transition Soft Actuator with Four Elements

Figure 4 shows the results of experiments for a multistable actuator comprising four bistable elements ($N = 4$). In this case, the number of binary states is 16, the number of intermediate states is 32, and the number of complete-cycle trajectories is 576, see Figure 4a. Similar to the previous set of experiments, the bistable elements are designed and fabricated with variability in their critical forces F^{\min} and F^{\max} , and connected as a serial chain, ordered from weaker to stronger, see Figure 4b. The four-element actuator setup is similar to the two-element actuator setup described above. Since the number of possible trajectories is extremely large, we present in Figure 4d the results for experimentally achieving four representative trajectories with a single input;

these experiments are also shown in the Supporting Information Video. Nevertheless, the ability to follow any other trajectory has been demonstrated both experimentally and numerically (in simulations), by choosing the appropriate input rate at every state transition. Each plot in Figure 4c shows the time response (elongation versus time) of individual elements in a complete extension stage from state (0000) to state (1111). The only difference between these experiments is the time-varying input rate $\nu(t)$ at which the system is actuated. This induces a different order in which the elements are “snapping” in $0 \rightarrow 1$ transitions. After each transition, the input rate is changed in order to select the next element to snap.

2.4. Theoretical Modeling and Analysis

We now present theoretical model and analysis of the multi-state actuator, which enables understanding the fundamental principles of our concept, as well as insightful guidelines for its design.

The multistate actuator is modeled as a set of N bistable elements connected in series, whose endpoints are attached to N linear rate-dependent dampers, as illustrated in Figure 1. The elastic force acting on each bistable element is dictated by its force–displacement relationship, $F_i(\epsilon_i)$. The dynamic equations of motion describing the response of the system are given in vector form as:

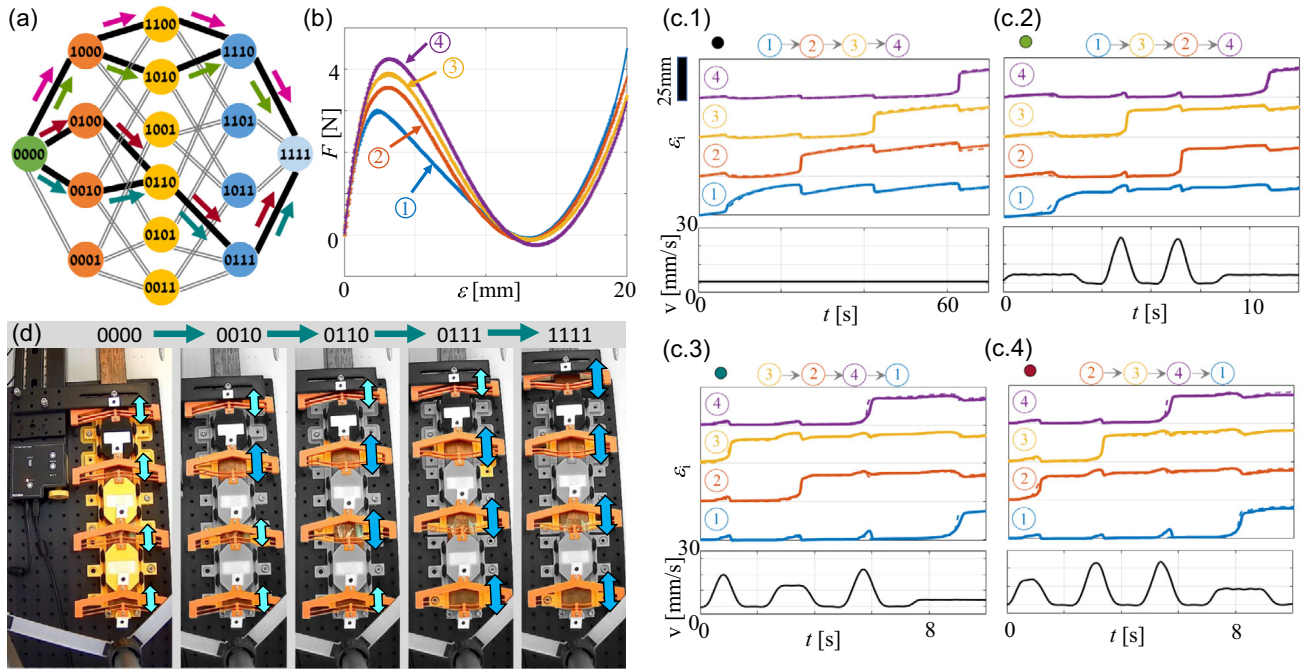


Figure 4. A multistable actuator with four bistable elements. a) Diagram with all possible binary states and transitions (not including intermediate ‘s’ states). Each colored sequence of arrows indicates a different order of the snapping sequence, obtained experimentally. b) The measured force–displacement profiles of the four elements, which were designed with ordered variability. c) Plots of four time responses, each associated with a different experiment and a different snap-through sequence (see colored arrows in (a) corresponding to the colored circles in (c.1) through (c.4)), showing the elongation, $\varepsilon_i(t)$, of each of the bistable elements in a complete extension from state (0000) to state (1111). Different choice of time-varying input rate of extension $v(t)$, shown in the bottom graphs. Thus, each experiment results in a different trajectory with a chosen order of elements’ snapping. d) Snapshots from the experiment for which the order of snapping elements is $\{3 \rightarrow 2 \rightarrow 4 \rightarrow 1\}$. That is, the sequence of binary state transitions is (0000) \rightarrow (0010) \rightarrow (0110) \rightarrow (0111) \rightarrow (1111). The small and large arrows in the pictures mark the closed and snapped-open elements, respectively.

$$\frac{d\boldsymbol{\varepsilon}}{dt} = \mathbf{W}\mathbf{F}(\boldsymbol{\varepsilon}) + \mathbf{v} \quad (2)$$

where $\boldsymbol{\varepsilon}(t) = [\varepsilon_1, \dots, \varepsilon_N]^T$, $\mathbf{F}(\boldsymbol{\varepsilon}) = [F_1(\varepsilon_1), F_2(\varepsilon_2), \dots, F_N(\varepsilon_N)]^T$, and \mathbf{W} is a tri-diagonal matrix which is given explicitly in Equation (S2), Supporting Information. Moreover, $\mathbf{v}(t) = [0, 0, \dots, 0, v(t)]^T$ with $v(t) = \dot{L}(t)$ being the extension rate of the chain, which is the controlled input.

This set of ordinary differential equations (ODEs) is inherently nonlinear due to the non-monotonic force–displacement relation of the bistable elements $F_i(\varepsilon_i)$. Thus, Equation (2) can be integrated numerically using a standard ODE solver in order to obtain the time response. Still, it is desired to gain some analytical insights and intuition. To this end, we replace the bistable force–displacement relation with a tri-linear profile, as illustrated in Figure 1c. This approximation preserves the main features of the bistable behavior, namely two phases of positive stiffness separated by a branch of negative stiffness, yet transforms the equations of motion into a set of piecewise-linear ODEs. More specifically, the governing equations are linear as long as the actuator’s state has not changed, and nonlinearity is merely introduced by the change of states.^[120,121] This important simplification enables analytical treatment, as discussed below.

2.4.1. Analysis of Actuator Dynamics with Two Bistable Elements

Next, we examine the behavior of the simplest multistate actuator, namely a system with two bistable elements, $N = 2$. In this case, equilibrium states and solutions of the actuator’s dynamic response can be easily visualized as curves in the plane of relative displacements $(\varepsilon_1, \varepsilon_2)$.

The equilibrium curves of a system with two identical bistable elements, $N = 2$, having the same force–displacement relation $F_i(\varepsilon_i)$, are shown in Figure 5a. Unstable equilibrium points are denoted as dashed curves, whereas stable equilibria are shown as solid curves. The red straight-line segments represent equilibrium curves obtained while approximating $F_i(\varepsilon_i)$ by a tri-linear function, as illustrated in Figure 1c, where each straight segment represents a different state of the system (e.g., (01), (1s), and so on), being stable or unstable. The array of short arrows in Figure 5a represent the vector field $d\boldsymbol{\varepsilon}/dt = \mathbf{W}\mathbf{F}(\boldsymbol{\varepsilon})$ under zero input $\mathbf{v} = \mathbf{0}$ when starting from non-equilibrium initial values. Thus, solution trajectories move along lines of constant total length, $\varepsilon_1 + \varepsilon_2 = L_0$, that is, in angle of -45° , in a direction that is repelled from unstable equilibrium branches and attracted toward stable ones. The stability of equilibrium branches corresponding to intermediate states $\{(0s), (s0), (1s), (s1)\}$ is determined as follows.

If the systems in Figure 5a,b move quasi-statically while slowly increasing the total length L above ε_{\max} for leaving (00) state, the

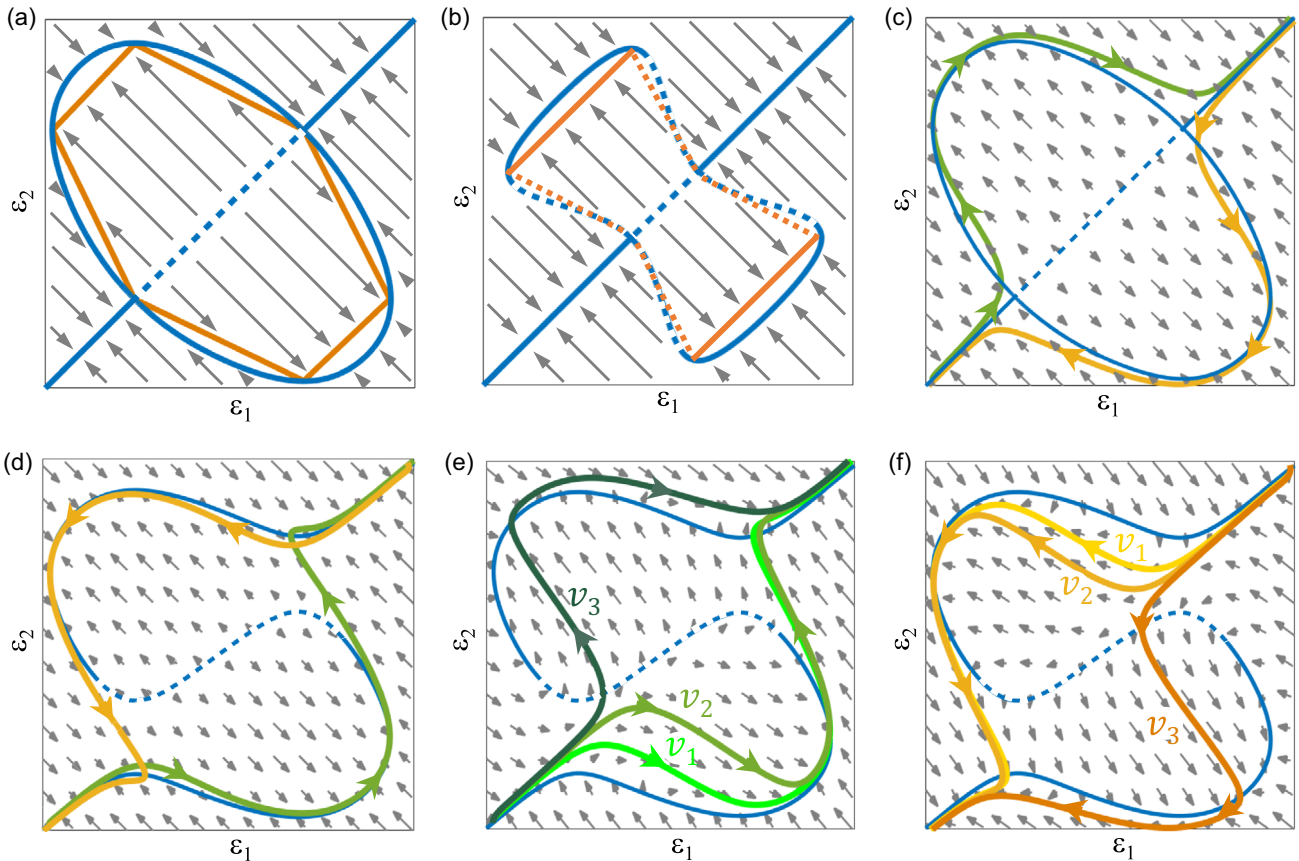


Figure 5. Illustrative maps of equilibrium curves in $(\varepsilon_1, \varepsilon_2)$ plane for multistable actuators with $N = 2$ elements. The grid of arrows describes the vector field of solution trajectories, repelled from unstable equilibrium curves (dashed) toward stable equilibria (solid lines). a) Two identical elements, with stable intermediate states $\{(0s), (s0), (1s), (s1)\}$. Blue curves correspond to polynomial profile $F(\varepsilon)$, whereas red line segments correspond to its tri-linear approximation. b) Case where the intermediate states are unstable equilibria. c) The arrowed curves denote trajectories under small input rate, green color - extension $\nu > 0$; orange color - contraction $\nu < 0$. The damping forces break symmetry and enable a non-reversible cycle of state transitions sequence $(00) \rightarrow (01) \rightarrow (11) \rightarrow (00)$, as in.^[1] d) With ordered variance between the elements as in (1). The symmetry is broken and equilibrium curves change topology, such that element 1 snaps first in slow extension (green arrowed trajectory) and element 2 snaps first in slow contraction (orange arrowed trajectory). e) Solution trajectories of extension $\nu > 0$, starting from state (00) with different input rates $\nu_1 < \nu_2 < \nu_3^+ < \nu_3$. The high input rate ν_3 which is beyond the critical rate ν_c^+ , changes the vector field $d\varepsilon/dt$ so that the trajectory can pass the “ridge line” of unstable equilibrium and fall into basin of attraction of state (10) , thus changing the order of snapping. f) Solution trajectories of contraction $\nu < 0$, starting from state (11) with different input rates $|\nu_1| < |\nu_2| < |\nu_3^-| < |\nu_3|$. The highest contraction rate ν_3 induces change in the order of snapping.

choice of transition to the next stable equilibrium state, that is, which elements is snapping first, is made at random, due to symmetry of the elements. However, for small input velocity, the damping forces break this symmetry and enforces a choice of state transitions. This is illustrated in Figure 5c, which shows the equilibrium curves for the same identical elements as in Figure 5a, while the arrowed curves represent near-equilibrium solution trajectories of $\varepsilon_i(t)$ under small input velocity, $\nu > 0$ for extension from (00) to (11) states, and $\nu < 0$ for contraction back from (11) to (00) , achieving a non-reversible cycle, as in.^[1]

In order to enable a controlled choice between state transitions, we now introduce a second symmetry-breaking mechanism of *designed variability* between the force–displacement relations of the elements, $F_i(\varepsilon_i)$. In particular, the variability is manifested by changing the critical forces F^{\max} and F^{\min} for each element, such that the second element is “weaker” than the first

one both in extension and contraction, as given in Equation (1). The equilibrium curves for such case in $(\varepsilon_1, \varepsilon_2)$ -plane appear in Figure 5d (unstable branches in dashed curves), illustrating that the symmetry is broken. The colored arrowed curves represent solution trajectories under small input $\nu > 0$ for extension from state (00) , followed by $\nu < 0$ for contraction back from (11) . One can see that the trajectories are closely following the stable equilibrium curves, and then a rapid “snap” occurs when the stable equilibrium branch ends, where the solution is repelled and then attracted to a different stable branch. This illustrates a state transition sequence $(00) \rightarrow (10) \rightarrow (11) \rightarrow (01) \rightarrow (00)$.

Next, we consider the effect of increasing the input rate ν . Assuming for simplicity that ν remains constant during extension, we show that there exists a critical rate,

$$\nu_c^+ \sim 2(F_2^{\max} - F_1^{\max})/c \quad (3)$$

such that for $v > v_c^+$ the state transition $(00) \rightarrow (10)$ changes to $(00) \rightarrow (01)$. This can be explained by visualizing the vector fields in (ϵ_1, ϵ_2) -plane. For very small input rate, the vector field is close to that in Figure 5d, and the solution trajectory follows closely the continuous stable equilibrium branch of $(00) \rightarrow (10)$. According to the system's dynamic Equation (2), increasing v adds the constant upward vector $[0, v]^T$ to the vector field at each point. Figure 5e shows solution trajectories $\epsilon_i(t)$ under three different input rates $v_1 < v_2 < v_c^+ < v_3$, where the vector field is shown for $v = v_3 > v_c^+$. One can see how the vector field is rotated and drives the solution upwards. A similar situation occurs in Figure 5f for contraction from state (11) with three input rates $v = v_j < 0$, such that $|v_1| < |v_2| < |v_c^-| < |v_3|$, with a different critical rate,

$$v_c^- \sim 2(F_2^{\min} - F_1^{\min})/c < 0 \quad (4)$$

For $v = v_3$, the vector field has an added downward component which enables the trajectory to leave the (11) branch and cross to (10). **Table 1** gives a comparison of the critical input rates v_c for $v > 0$ and $v < 0$, calculated from Equation (3) to (4) and (S5), Supporting Information under tri-linear approximation, as well as from numerical integration of Equation (2) assuming polynomial profiles for $F_i(\epsilon_i)$, as fitted from experiments. The last row in Table 1 gives the actual critical input rates as obtained from experiments shown in Figure 2. For more mathematical details see Section B in the Supporting Information.

2.4.2. Analysis of Actuator Dynamics with Three Bistable Elements

By similar considerations as those applied in the analysis of a system with two bistable elements, one can directly generalize the concept to a multistable actuator with three elements. To this end, pre-designed variability is introduced to the bistable behavior of the elements, and the elements are arranged in series from weaker to stronger, as formulated in Equation (1) and illustrated in Figure 1d.

In this case, state (111) can be reached through six distinct trajectories that all begin from state (000), see **Figure 6**. These trajectories are achieved in two separate steps. First, one element snaps, resulting in one of the three intermediate states (100), (010), or (001). In the second step, another element snaps, leading to the states (110), (101), or (011). After these two steps, any additional extension ($v > 0$) will drive the system to the final state (111).

During the first step, when the input rate of extension v is very low, all elements experience almost the same force, causing the weakest element to snap first and transition from state '0' to '1'. This results in the trajectory $(000) \rightarrow (100)$. For higher input rates, the force distribution becomes more uneven, with rate-dependent terms becoming more pronounced for elements located closer to the actuated end of the chain. A critical rate

Table 1. Magnitudes of the critical input rate $|v_c|$ in $[\text{mm s}^{-1}]$ for the two-elements system considered in Figure S1, Supporting Information. Row 1 - Using tri-linear functions for approximating measured profiles $F_i(\epsilon_i)$ and the asymptotic approximation in Equation (S6). Row 2 - Using tri-linear functions and solving the transcendental Equation (S5). Row 3 - Using fitted polynomial profiles $F_i(\epsilon_i)$ and iterative numerical integration of the nonlinear dynamic Equation (2). Row 4 - actual values from experimental measurements for iteratively obtaining changes in state transition, with standard deviations indicated. The results demonstrate the predictive power of the theoretical model and its simplified approximations.

No.	Critical input rate $ v_c $	Extension $v > 0$	Contraction $v < 0$
1.	Asymptotic approximation from Equation (3) to (4)	26.17	27.51
2.	Analytical approximation from Equation (S9)	26.44	27.79
3.	Integration of Equation (2) for polynomial profile	25.59	26.30
4.	Experimental results	25 ± 1	27.5 ± 1.5

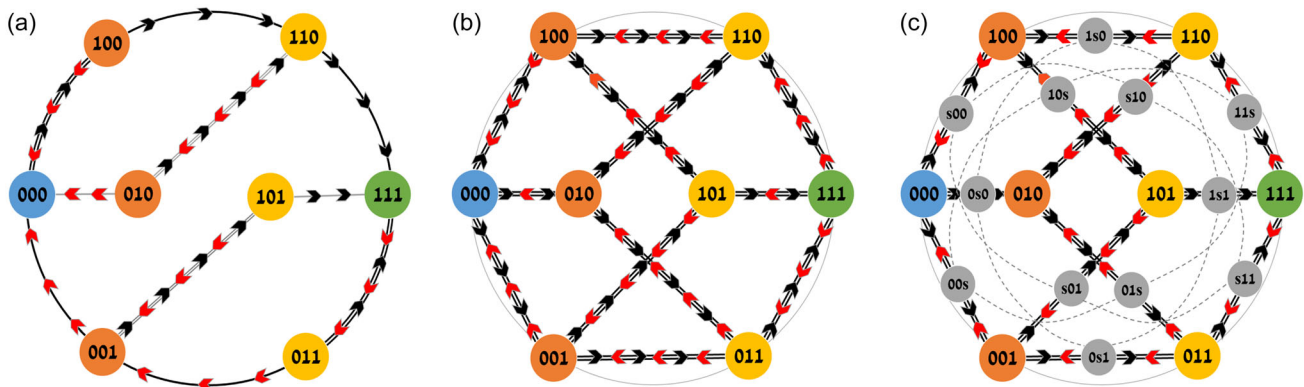


Figure 6. Examples of several state transition diagrams for a multistate actuator with $N = 3$ bistable elements, which offers 8 (or 2^N) possible binary states. a) State-of-the-art single-input actuators with ordered variability or dissipative damping as in^[1] enable reaching any state, but the sequence of quasi-static transitions from initial to target state is limited to a specific order, which results in long, often impractical, sequences. b) Single-input multiple-transition actuator. Our concept enables following any desired complete-cycle trajectory with a single input. The number of complete-cycle trajectories is 36 for $N = 3$ (generally $(N!)^2$). c) High-resolution single-input multiple-transition actuator, where intermediate states having one element at 's' phase are deliberately designed to be stable, enabling enhanced trajectory resolution with 20 stable states for $N = 3$ (generally $2^{N-1}(N+2)$).

Table 2. Six trajectories derived from the actuator dynamics of three bistable elements, along with their corresponding critical velocities. For brevity, we denote $\Delta F_{ij} = F_i^{\max} - F_j^{\max}$.

First step input rate region	
(000) \rightarrow (100)	$\nu < 3\Delta F_{21}/c$
(000) \rightarrow (010)	$3\Delta F_{21}/c < \nu < 3\Delta F_{32}/2c$
(000) \rightarrow (001)	$\nu > 3\Delta F_{32}/2c$
Second step input rate region	
(100) \rightarrow (110)	$\nu < 3\Delta F_{32}/2c$
(100) \rightarrow (101)	$\nu > 3\Delta F_{32}/2c$
(010) \rightarrow (110)	$\nu < \Delta F_{13}/c$
(010) \rightarrow (011)	$\nu > \Delta F_{13}/c$
(001) \rightarrow (101)	$\nu < 3\Delta F_{13}/c$
(001) \rightarrow (011)	$\nu > 3\Delta F_{13}/c$

exists above which the next element snaps first to phase ‘1’, resulting in the trajectory (000) \rightarrow (010). This rate is approximately given by $\nu_{c,1}^+ \sim 3(F_2^{\max} - F_1^{\max})/c$. At even higher rates, the third element may snap first, leading to the trajectory (000) \rightarrow (001). A separate critical rate exists for this transition, represented as $\nu_{c,2}^+ \sim 3(F_3^{\max} - F_2^{\max})/2c$.

The second step depends on the binary state reached in the chain after the first step. However, the analysis in the second step follows a similar pattern to that of the first step. There are three critical rates that determine the possible transitions. The six trajectories, along with their corresponding critical input rate, are summarized in the **Table 2**.

2.4.3. *N* Elements

By applying similar principles to that used in the analysis of systems with two and three bistable elements, the concept can be directly extended to a multistable actuator with *N* elements.

Consider a given stable equilibrium state. Under a very low input rate of extension $\nu > 0$, all elements experience (almost) the same level of force; thus, the weakest element is the first to snap and change its phase from ‘0’ to ‘1’. For higher input rate, the distribution of forces becomes less uniform, adding rate-dependent terms which become larger for elements located closer to the chain’s actuated end. Thus, there is a critical rate above which the next element snaps first to phase ‘1’, and a higher rate that can make a farther element to snap first. The same principle applies also for contraction input $\nu < 0$, and for stable intermediate states. That is, every transition between two stable states, as those shown in the state diagrams in Figure 2i, 3a, 4a, and 6, can be associated with an interval of input rates ν under which this transition is achieved. However, for $N > 3$, explicit analysis as shown above for $N = 2, 3$ becomes more complicated, and the critical input rates that determine each state transition can only be obtained using numerical integration of the actuator’s nonlinear dynamic Equation (2) using

fitted polynomial profiles for $F_i(e_i)$, as done in our experimental demonstration with $N = 4$ shown in Figure 4.

3. Materials and Methods

3.1. Fabrication of Bistable Elements

The bi-stable elements were made of PLA and fabricated using a 3D-printer Ultimaker 5s. Each element consists of two parallel pairs of clamped-clamped bending beams with locally varying thicknesses, as shown in Figure S1b, Supporting Information. The geometry and thickness profiles of the beams were designed in order to create the desired bistable force–displacement profiles.

In order to characterize the force–displacement relation of each bistable element, we have applied standard elongation and contraction tests using Instron measurement system, as shown in Figure S1c, Supporting Information. The output of the system gives data points of force measurements versus displacement. The discrete points obtained from measurements under four extension-contraction cycles, were then fitted by a 5th-order polynomial, as shown in Figure S1d, Supporting Information. The polynomial fit has also been used to extract the values at extremum points $\{\epsilon_{\min}, \epsilon_{\max}, F_{\min}, F_{\max}\}$, which were then used in order to approximate the tri-linear profile, as shown in Figure 1b.

3.2. Experimental Setup

3.2.1. Actuator

The bistable elements have been serially connected to 3D-printed wheeled carts, moving on a supporting rail. In order to obtain large viscous damping, the cart has been equipped with a strong magnetic block, while an elongated copper plate (thickness 13 mm) has been mounted to the rail, under the carts. The moving endpoint of the chain of elements has been connected to an arm that moves on a track, actuated by a lead screw connected to a stepper motor (HANPOSE 23H65628), which is commanded by a microcontroller, in order to obtain fixed-rate elongation or contraction of a chain of *N* elements. The motion of the elements and the arm have been captured using a digital camera mounted on top of the setup. Marker stickers on the elements were detected and tracked using Matlab image processing toolbox, in order to obtain time series of the elongation of each element.

3.2.2. 3-link Robot

The 3-link robot has been mounted on the cart connecting two bistable elements, as shown in Figure 3. Each side link of the robot has been connected to a bistable element by a ‘<’-shaped coupling link connected at its endpoints to passive joints. The dimensions of the coupling link and location of its connection points were designed such that the open, closed states of the bistable element result in elbow up, down angles of the robot’s side links, respectively. The robot’s links and their connecting joints were made of ABS, and 3D-printed using Ultimaker 5 s printer.

3.3. Numerical Analysis of the System's Dynamics

We have created a computational simulation code for the numerical integration of the N-element system's coupled nonlinear dynamic Equation (2). The integration was performed in Matlab using the 'ode45' adaptive-step integrator. The force-displacement relations of the simulated elements were based on the 5th-degree polynomials fitted from experimental measurements. The value of the damping coefficient in the experiments was extracted from preliminary calibration experiments of magnetic force measurements, and was estimated as $c = 15 \text{ Ns m}^{-1}$. The numerical code enables analyzing equilibrium states of the N-element systems, as well as their stability. In addition, it enables numerically finding critical values of input rate of the total chain elongation/contraction that result in changing the order of state transitions, as well as their dependence on the bi-stability profiles of the elements. We have used the simulation code in order to design properties of our N-element systems for achieving desired sequences of state transitions.

4. Discussion and Conclusions

We presented a novel concept that paves the way for realizing a new class of robotic actuation and sets the stage for the next-generation of soft robots with minimal control and maximal dexterity. This is accomplished by exploiting the unique dynamic behavior of multistable elastic structures that are comprised from an array of mechanically coupled bistable elements. By combining rate-dependent dissipation at the single-element level with carefully and cleverly pre-designed differences in the bistable behavior of the elements, we are able to facilitate any desired multistate transition using a *single* dynamic input.

Our experiments showed that we can choose between any desired trajectory out of 576 possible ones with a 4-DOFs system, using a single control input. The actual use of such single-input control actuator was demonstrated by connecting it to a 3-link robot, representing a Purcell's swimmer or a simple snake-like robot, where it was illustrated that it provides any desired functional deformation cycle with a single input. Importantly, the proposed concept can be realized at any practical scale and it does not require activation by external (e.g., magnetic or electric) fields. The latter is particularly important since the employment of such fields may restrict the use of the actuator due to potential interference with sensitive electronics or optical components. Our extensive analysis, based on theoretical, numerical, and experimental study, has validated the feasibility and applicability of this concept, and provided important insights and guidelines regarding the design of such multistate actuators. It was also shown that the extraordinary ability to choose any desired sequence of state-transitions can be directly extended to any number of DOFs, enabling the control over a very large number of possible trajectories, which goes as $(N!)^2$ where N is the number of DOFs, with a *single* controlled input.

Although these promising results highlight the potential of our approach, several key directions remain for future research. First, it is necessary to demonstrate the proposed concept on additional robots with multiple DOFs, particularly those designed for industrial applications. Additionally, the dissipation

mechanism should be generalized to be an integral part of the robot's soft structure, rather than relying on external rigid components such as magnets. Another important step is to incorporate the actuator and its bistable element network directly within the robot's structure, further enhancing its integration and efficiency. Finally, exploring more complex interconnections between the elements—potentially evolving into a “learning network”—could open new possibilities for adaptive and intelligent actuation.^[122] These future advancements will further strengthen the potential of our approach, pushing the boundaries of soft robotics, multistable actuators, and single-input control strategies.

Supporting Information

Supporting Information is available from the Wiley Online Library or from the author.

Acknowledgements

S.G. acknowledges support from the Israel Science Foundation (grant no. 1598/21). The work of Y.O. and A.G. was supported by the PMRI – Peter Munk Research Institute – Technion, under (grant no. 2031886), and the Technion Autonomous Systems Program under (grant no. 2031975).

Conflict of Interest

The authors declare no conflict of interest.

Author Contributions

Geron Yomit: formal analysis (equal); investigation (supporting); methodology (equal); software (supporting); validation (lead); visualization (supporting). **Ben-Haim Eran:** formal analysis (equal); investigation (lead); software (lead); validation (supporting); visualization (supporting); writing—original draft (supporting); writing—review & editing (lead). **Gat D. Amir:** conceptualization (supporting); formal analysis (supporting); funding acquisition (lead); investigation (supporting); methodology (supporting); project administration (supporting); resources (supporting); supervision (lead); writing—review & editing (supporting). **Or Yizhar:** conceptualization (lead); formal analysis (supporting); funding acquisition (lead); investigation (supporting); methodology (lead); project administration (supporting); resources (lead); supervision (lead); validation (supporting); visualization (equal); writing—original draft (lead); writing—review & editing (equal). **Civli Sefi:** conceptualization (lead); formal analysis (supporting); funding acquisition (lead); investigation (supporting); methodology (lead); project administration (supporting); resources (lead); supervision (lead); validation (supporting); visualization (equal); writing—original draft (lead); writing—review & editing (equal). **Geron Yomit and Ben-Haim Eran** contributed equally to this work.

Data Availability Statement

The data that support the findings of this study are available in the Supporting Information of this article.

Keywords

bistable, harnessing structural instabilities, multi-stable, single-input control, soft robotics

Received: February 13, 2025
Published online:

- [1] E. Ben-Haim, L. Salem, Y. Or, A. D. Gat, *Soft Robot.* **2020**, 7, 259.
- [2] B. Gorissen, D. Melancon, N. Vasios, M. Torbati, K. Bertoldi, *Sci. Robot.* **2020**, 5, eabb1967.
- [3] K. M. Lynch, F. C. Park, *Modern Robotics*, Cambridge University Press, Cambridge **2017**.
- [4] S. B. Niku, *Introduction to Robotics: Analysis, Control, Applications*, John Wiley & Sons, Hoboken, NJ **2020**.
- [5] Z. Shen, F. Chen, X. Zhu, K.-T. Yong, G. Gu, *J. Mater. Chem. B* **2020**, 8, 8972.
- [6] R. F. Shepherd, F. Ilievski, W. Choi, S. A. Morin, A. A. Stokes, A. D. Mazzeo, X. Chen, M. Wang, G. M. Whitesides, *Proc. Natl. Acad. Sci.* **2011**, 108, 20400.
- [7] A. D. Marchese, R. K. Katzschnmann, D. Rus, *Soft Robot.* **2015**, 2, 7.
- [8] Y. Tang, Y. Li, Y. Hong, S. Yang, J. Yin, *Proc. Natl. Acad. Sci.* **2019**, 116, 26407.
- [9] Y. Lee, W. J. Song, J.-Y. Sun, *Mater. Today Phys.* **2020**, 15, 100258.
- [10] J. Cao, C. Zhou, G. Su, X. Zhang, T. Zhou, Z. Zhou, Y. Yang, *Adv. Mater.* **2019**, 31, 1900042.
- [11] K. Park, J. Ha, B. Shin, H.-Y. Kim, *Soft Matter in Plants: From Biophysics to Biomimetics*, Royal Society of Chemistry, Cambridge, England **2022**.
- [12] S. Palagi, A. G. Mark, S. Y. Reigh, K. Melde, T. Qiu, H. Zeng, C. Parmeggiani, D. Martella, A. Sanchez-Castillo, N. Kapernaum, F. Giesselmann, D. S. Wiersma, E. Lauga, P. Fischer, *Nat. Mater.* **2016**, 15, 647.
- [13] M. Rogó, H. Zeng, C. Xuan, D. S. Wiersma, P. Wasylczyk, *Adv. Opt. Mater.* **2016**, 4, 1689.
- [14] M. Pilz Da Cunha, M. G. Debije, A. P. H. J. Schenning, *Chem. Soc. Rev.* **2020**, 49, 6568.
- [15] Y. Bar-Cohen, *J. Spacecr. Rockets* **2002**, 39, 822.
- [16] Y. Wu, J. K. Yim, J. Liang, Z. Shao, M. Qi, J. Zhong, Z. Luo, X. Yan, M. Zhang, X. Wang, R. S. Fearing, R. J. Full, L. Lin, *Sci. Robot.* **2019**, 4, eaax1594.
- [17] G. Z. Lum, Z. Ye, X. Dong, H. Marvi, O. Erin, W. Hu, M. Sitti, *Proc. Natl. Acad. Sci.* **2016**, 113, E6007.
- [18] S. Wu, W. Hu, Q. Ze, M. Sitti, R. Zhao, *Multifunct. Mater.* **2020**, 3, 042003.
- [19] L. Hines, K. Petersen, G. Z. Lum, M. Sitti, *Adv. Mater.* **2017**, 29, 1603483.
- [20] N. El-Atab, R. B. Mishra, F. Al-Modaf, L. Joharji, A. A. Alsharif, H. Alamoudi, M. Diaz, N. Qaiser, M. M. Hussain, *Adv. Intell. Syst.* **2020**, 2, 2000128.
- [21] S. Coyle, C. Majidi, P. LeDuc, K. Jimmy Hsia, *Extreme Mech. Lett.* **2018**, 22, 51.
- [22] A. Pal, V. Restrepo, D. Goswami, R. V. Martinez, *Adv. Mater.* **2021**, 33, 2006939.
- [23] Y. Cao, M. Derakhshani, Y. Fang, G. Huang, C. Cao, *Adv. Funct. Mater.* **2021**, 31, 2106231.
- [24] V. K. Venkiteswaran, L. F. P. Samaniego, J. Sikorski, S. Misra, *IEEE Robot. Autom. Lett.* **2019**, 4, 1753.
- [25] E. C. Goldfield, Y.-L. Park, B.-R. Chen, W.-H. Hsu, D. Young, M. Wehner, D. G. Kely-Stephen, L. Stirling, M. Weinberg, D. Newman, R. Nagpal, E. Saltzman, K. G. Holt, C. Walsh, R. J. Wood, *Ecol. Psychol.* **2012**, 24, 300.
- [26] A. D. Marchese, C. D. Onal, D. Rus, *Soft robotics* **2014**, 1, 75.
- [27] J. Shintake, V. Cacucciolo, D. Floreano, H. Shea, *Adv. Mater.* **2018**, 30, 1707035.
- [28] W. Wang, S.-H. Ahn, *Soft Robot.* **2017**, 4, 10.
- [29] Z. Ren, R. Zhang, R. Soon, Z. Liu, W. Hu, P. Onck, M. Sitti, *Sci. Adv.* **2021**, 7, eabh2022.
- [30] M. T. Petralia, R. J. Wood, in *2010 IEEE/RSJ Int. Conf. on Intelligent Robots and Systems*, IEEE, Piscataway, NJ **2010**, pp. 2357–2363.
- [31] Q. Wang, Z. Wu, J. Huang, Z. Du, Y. Yue, D. Chen, D. Li, B. Su, *Composites, Part B* **2021**, 223, 109116.
- [32] W. Zhang, P. Polygerinos, in *2018 Annual American Control Conf. (ACC)*, Milwaukee, WI **2018**, pp. 2096–2101.
- [33] L. Ren, B. Li, G. Wei, K. Wang, Z. Song, Y. Wei, L. Ren, Q. Liu, *iScience* **2021**, 24, 103075.
- [34] B. He, Y. Zhou, Z. Wang, Q. Wang, R. Shen, S. Wu, *Sens. Actuators, A* **2018**, 272, 341.
- [35] S. A. Morin, Y. Shevchenko, J. Lessing, S. W. Kwok, R. F. Shepherd, A. A. Stokes, G. M. Whitesides, *Adv. Mater.* **2014**, 26, 5991.
- [36] S. A. Morin, S. W. Kwok, J. Lessing, J. Ting, R. F. Shepherd, A. A. Stokes, G. M. Whitesides, *Adv. Funct. Mater.* **2014**, 24, 5541.
- [37] N. W. Bartlett, M. T. Tolley, J. T. B. Overvelde, J. C. Weaver, B. Mosadegh, K. Bertoldi, G. M. Whitesides, R. J. Wood, *Science* **2015**, 349, 161.
- [38] B. C. Mac Murray, X. An, S. S. Robinson, I. M. van Meerbeek, K. W. O'Brien, H. Zhao, R. F. Shepherd, *Adv. Mater.* **2015**, 27, 6334.
- [39] M. De Volder, J. Peirs, D. Reynaerts, J. Coosemans, R. Puers, O. Smal, B. Raucourt, *J. Micromech. Microeng.* **2005**, 15, S15.
- [40] T. Li, G. Li, Y. Liang, T. Cheng, J. Dai, X. Yang, B. Liu, Z. Zeng, Z. Huang, Y. Luo, T. Xie, W. Yang, *Sci. Adv.* **2017**, 3, e1602045.
- [41] E. Acome, S. K. Mitchell, T. G. Morrissey, M. B. Emmett, C. Benjamin, M. King, M. Radakovitz, C. Keplinger, *Science* **2018**, 359, 61.
- [42] M. Shahinpoor, Y. Bar-Cohen, J. O. Simpson, J. Smith, *Smart Mater. Struct.* **1998**, 7, R15.
- [43] A. Punning, S. Akbari, M. Niklaus, H. Shea, *Electroactive Polymer Actuators and Devices (EAPAD) 2011*, Vol. 7976, SPIE, Bellingham, Washington **2011**, pp. 259–266.
- [44] G. Mao, M. Drack, M. Karami-Mosammam, D. Wirthl, T. Stockinger, R. Schwödlauer, M. Kaltenbrunner, *Sci. Adv.* **2020**, 6, eabc0251.
- [45] Y. Kim, H. Yuk, R. Zhao, S. A. Chester, X. Zhao, *Nature* **2018**, 558, 274.
- [46] W. Hu, G. Z. Lum, M. Mastrangeli, M. Sitti, *Nature* **2018**, 554, 81.
- [47] R. Fuhrer, E. K. Athanassiou, N. A. Luechinger, W. J. Stark, *Small* **2009**, 5, 383.
- [48] Y. He, J. Tang, Y. Hu, S. Yang, F. Xu, M. Zrnyi, Y. Mei Chen, *Chem. Eng. J.* **2023**, 462, 142193.
- [49] Q. He, Z. Wang, Y. Wang, A. Minori, M. T. Tolley, S. Cai, *Sci. Adv.* **2019**, 5, eaax5746.
- [50] Y. Zhao, Y. Chi, Y. Hong, Y. Li, S. Yang, J. Yin, *Proc. Natl. Acad. Sci.* **2022**, 119, e2200265119.
- [51] Y. Li, Y. Teixeira, G. Parlato, J. Grace, F. Wang, B. D. Huey, X. Wang, *Soft Matter* **2022**, 18, 6857.
- [52] C. Stergiopoulos, D. Vogt, M. T. Tolley, M. Wehner, J. Barber, G. M. Whitesides, R. J. Wood, *Smart Materials, Adaptive Structures and Intelligent Systems*, Vol. 46155V002T04A011, American Society of Mechanical Engineers, New York, NY **2014**.
- [53] R. F. Shepherd, A. A. Stokes, J. Freake, J. Barber, P. W. Snyder, A. D. Mazzeo, L. Cademartiri, S. A. Morin, G. M. Whitesides, *Angew. Chem., Int. Ed.* **2013**, 52, 2892.
- [54] M. T. Tolley, R. F. Shepherd, M. Karpelson, N. W. Bartlett, K. C. Galloway, M. Wehner, R. Nunes, G. M. Whitesides, R. J. Wood, in *2014 IEEE/RSJ Int. Conf. on Intelligent Robots and Systems*, IEEE, Piscataway, NJ **2014**, pp. 561–566.
- [55] S. Wu, G. L. Baker, J. Yin, Y. Zhu, *Soft Robot.* **2022**, 9, 1031.
- [56] S. Wu, Y. Hong, Y. Zhao, J. Yin, Y. Zhu, *Sci. Adv.* **2023**, 9, ead8014.
- [57] M. Vangbo, *Sens. Actuators, A* **1998**, 69, 212.
- [58] J. Zhao, J. Jia, X. He, H. Wang, *J. Appl. Mech.* **2008**, 75, 041020.
- [59] R. V. Mises, *J. Appl. Math. Mech./Zeitschrift für Angewandte Mathematik und Mechanik* **1923**, 3, 406.

- [60] G. Arena, R. M. J. Groh, A. Brinkmeyer, R. Theunissen, P. M. Weaver, A. Pirrera, *Proc. R. Soc. A: Math. Phys. Eng. Sci.* **2017**, 473, 20170334.
- [61] S. P. Timoshenko, J. M. Gere, *Theory of Elastic Stability*, Courier Corporation, North Chelmsford, MA **2009**.
- [62] H. Alexander, *Int. J. Eng. Sci.* **1971**, 9, 151.
- [63] I. Müller, P. Strehlow, *Rubber and Rubber Balloons: Paradigms of Thermodynamics*, Vol. 637, Springer Science & Business Media, Berlin **2004**.
- [64] J. T. B. Overvelde, T. Kloek, J. J. A. D'haen, K. Bertoldi, *Proc. Natl. Acad. Sci.* **2015**, 112, 10863.
- [65] G. W. Brodland, H. Cohen, *Int. J. Solids Struct.* **1987**, 23, 1341.
- [66] D. P. Holmes, A. J. Crosby, *Adv. Mater.* **2007**, 19, 3589.
- [67] J. A. Faber, J. P. Udani, K. S. Riley, A. R. Studart, A. F. Arrieta, *Adv. Sci.* **2020**, 7, 2001955.
- [68] M. Taffetani, X. Jiang, D. P. Holmes, D. Vella, *Proc. R. Soc. A: Math. Phys. Eng. Sci.* **2018**, 474, 20170910.
- [69] S. D. Guest, S. Pellegrino, *Proc. R. Soc. A: Math. Phys. Eng. Sci.* **2006**, 462, 839.
- [70] S. Armon, E. Efrati, R. Kupferman, E. Sharon, *Science* **2011**, 333, 1726.
- [71] M. Gomez, D. E. Moulton, D. Vella, *Phys. Rev. Lett.* **2017**, 119, 144502.
- [72] M. Liu, L. Domino, I. Dupont de Dinechin, M. Taffetani, D. Vella, *J. Mech. Phys. Solids* **2023**, 170, 105116.
- [73] L. Shui, K. Ni, Z. Wang, *ACS Appl. Mater. Interfaces* **2022**, 14, 43802.
- [74] C. Keplinger, T. Li, R. Baumgartner, Z. Suo, S. Bauer, *Soft Matter* **2012**, 8, 285.
- [75] L. Dong, X. Tong, H. Zhang, M. Chen, Y. Zhao, *Mater. Chem. Front.* **2018**, 2, 1383.
- [76] S. Kim, C. Laschi, B. Trimmer, *Trends Biotechnol.* **2013**, 31, 287.
- [77] C. Majidi, *Soft Robot.* **2014**, 1, 5.
- [78] D. Rus, M. T. Tolley, *Nature* **2015**, 521, 467.
- [79] M. Cianchetti, C. Laschi, A. Menciassi, P. Dario, *Nat. Rev. Mater.* **2018**, 3, 143.
- [80] M. Cianchetti, T. Ranzani, G. Gerboni, T. Nanayakkara, K. Althoefer, P. Dasgupta, A. Menciassi, *Soft Robot.* **2014**, 1, 122.
- [81] C. Lee, M. Kim, Y. J. Kim, N. Hong, S. Ryu, H. Jin Kim, S. Kim, *Int. J. Control Autom. Syst.* **2017**, 15, 3.
- [82] Y. Chi, Y. Li, Y. Zhao, Y. Hong, Y. Tang, J. Yin, *Adv. Mater.* **2022**, 34, 2110384.
- [83] S. Katz, S. Givli, *Extreme Mech. Lett.* **2018**, 22, 106.
- [84] Y. Tang, Y. Chi, J. Sun, T.-H. Huang, O. H. Maghsoudi, A. Spence, J. Zhao, H. Su, J. Yin, *Sci. Adv.* **2020**, 6, eaaz6912.
- [85] T. Chen, O. R. Bilal, K. Shea, C. Daraio, *Proc. Natl. Acad. Sci.* **2018**, 115, 5698.
- [86] R. Baumgartner, A. Kogler, J. M. Stadlbauer, C. C. Foo, R. Kaltseis, M. Baumgartner, G. Mao, C. Keplinger, S. J. A. Koh, N. Arnold, Z. Suo, M. Kaltenbrunner, S. Bauer, *Adv. Sci.* **2020**, 7, 1903391.
- [87] Z. Jiao, C. Zhang, W. Wang, M. Pan, H. Yang, J. Zou, *Adv. Sci.* **2019**, 6, 1901371.
- [88] Z. Zhakypov, K. Mori, K. Hosoda, J. Paik, *Nature* **2019**, 571, 381.
- [89] B. Trembl, A. Gillman, P. Buskohl, R. Vaia, *Proc. Natl. Acad. Sci.* **2018**, 115, 6916.
- [90] D. J. Preston, P. Rothemund, H. J. Jiang, M. P. Nemitz, J. Rawson, Z. Suo, G. M. Whitesides, *Proc. Natl. Acad. Sci.* **2019**, 116, 7750.
- [91] D. Glozman, N. Hassidov, M. Senesh, M. Shoham, *IEEE Trans. Biomed. Eng.* **2010**, 57, 1264.
- [92] K. Che, C. Yuan, H. Jerry Qi, J. Meaud, *Soft Matter* **2018**, 14, 2492.
- [93] E. Milana, B. Van Raemdonck, A. S. Casla, M. De Volder, D. Reynaerts, B. Gorissen, *Front. Robot. AI* **2022**, 8, 788067.
- [94] M. Gude, W. Hufenbach, C. Kirvel, *Compos. Struct.* **2011**, 93, 377.
- [95] L. Medina, R. Gilat, S. Krylov, *Int. J. Eng. Sci.* **2017**, 110, 15.
- [96] X. Hou, Y. Liu, G. Wan, Z. Xu, C. Wen, H. Yu, J. X. J. Zhang, J. Li, Z. Chen, *Appl. Phys. Lett.* **2018**, 113, 221902.
- [97] R. L. Harne, M. Thota, K. W. Wang, *Appl. Phys. Lett.* **2013**, 102, 053903.
- [98] D. N. Betts, H. Alicia Kim, C. R. Bowen, D. J. Inman, *Appl. Phys. Lett.* **2012**, 100, 114104.
- [99] Z. Wang, X. Zhang, Y. Wang, Z. Fang, H. Jiang, Q. Yang, X. Zhu, M. Liu, X. Fan, J. Kong, *Adv. Sci.* **2023**, 10, 2206662.
- [100] P. Kaarthik, F. L. Sanchez, J. Avtges, R. L. Truby, *Soft Matter* **2022**, 18, 8229.
- [101] A. Zolfagharian, A. Kaynak, A. Kouzani, *Mater. Des.* **2020**, 188, 108411.
- [102] D.-A. Wang, J.-H. Chen, H.-T. Pham, *Sens. Actuators, A* **2013**, 189, 481.
- [103] S. Shan, S. H. Kang, J. R. Raney, P. Wang, L. Fang, F. Candido, J. A. Lewis, K. Bertoldi, *Adv. Mater.* **2015**, 27, 4296.
- [104] W. Ma, Z. Zhang, H. Zhang, Y. Li, H. Wu, S. Jiang, G. Chai, *Smart Mater. Struct.* **2019**, 28, 025028.
- [105] Y. Wu, R. Chaunsali, H. Yasuda, K. Yu, J. Yang, *Sci. Rep.* **2018**, 8, 112.
- [106] L. S. Novelino, Q. Ze, S. Wu, G. H. Paulino, R. Zhao, *Proc. Natl. Acad. Sci.* **2020**, 117, 24096.
- [107] J. Kaufmann, P. Bhowad, S. Li, *Soft Robot.* **2022**, 9, 212.
- [108] H. Son, Y. Park, Y. Na, C. Yoon, *Polymers* **2022**, 14, 4235.
- [109] A. Gillman, G. Wilson, K. Fuchi, D. Hartl, A. Pankonien, P. Buskohl, *Actuators* **2018**, 8, 3.
- [110] H. Yasuda, T. Tachi, M. Lee, J. Yang, *Nat. Commun.* **2017**, 8, 962.
- [111] B. Gorissen, E. Milana, A. Baeyens, E. Broeders, J. Christiaens, K. Collin, D. Reynaerts, M. De Volder, *Adv. Mater.* **2019**, 31, 1804598.
- [112] D. Melancon, A. E. Forte, L. M. Kamp, B. Gorissen, K. Bertoldi, *Adv. Funct. Mater.* **2022**, 32, 2201891.
- [113] G. Puglisi, L. Truskinovsky, *J. Mech. Phys. Solids* **2000**, 48, 1.
- [114] H. Hussein, P. Le Moal, R. Younes, G. Bourbon, Y. Haddab, P. Lutz, *Mech. Mach. Theory* **2019**, 131, 204.
- [115] G. Salinas, S. Givli, *Microsyst. Technol.* **2015**, 21, 943.
- [116] L. H. Cadwell, *Am. J. Phys.* **1996**, 64, 917.
- [117] L. E. Becker, S. A. Koehler, H. A. Stone, *J. Fluid Mech.* **2003**, 490, 15.
- [118] E. Kanso, J. E. Marsden, C. W. Rowley, J. B. Melli-Huber, *J. Nonlinear Sci.* **2005**, 15, 255.
- [119] B. Gamus, A. D. Gat, Y. Or, *IEEE Robot. Autom. Lett.* **2020**, 6, 111.
- [120] I. Benichou, S. Givli, *J. Mech. Phys. Solids* **2013**, 61, 94.
- [121] S. Nitecki, S. Givli, *J. Mech. Phys. Solids* **2021**, 157, 104634.
- [122] B.-H. Eran, G. Sefi, O. Yizhar, G. D. Amir, *Adv. Intell. Syst.* **2025**, 2400694.